REPORT DOCUMENTATION PAGE

Form Approved

AFRL-SR-AR-TR-09-0134

1. REPORT DATE (DD-MM-YYYY)	2. REPORT TYPE	3. DATES COVERED (From - To)
18-02-2009	Final Report	01-12-2005 – 30-11-2008

4. TITLE AND SUBTITLE
(U) Two-Point Scalar Time-Series Measurements in Turbulent

Partially Premixed Flames

5a. CONTRACT NUMBER

5b. GRANT NUMBER
FA9550-06-1-0064

5c. PROGRAM ELEMENT NUMBER
61102F

6. AUTHOR(S)
Galen B. King, Normand M. Laurendeau, and Michael W. Renfro

5d. PROJECT NUMBER
2308

5e. TASK NUMBER
BX

5f. WORK UNIT NUMBER

7. PERFORMING ORGANIZATION NAME(S) AND ADDRESS(ES)

School of Mechanical Engineering
Purdue University
West Lafayette, IN 47907-1288

Department of Mechanical Engineering
University of Connecticut
Storrs, CT 06269-3139

8. PERFORMING ORGANIZATION REPORT NUMBER

9. SPONSORING / MONITORING AGENCY NAME(S) AND ADDRESS(ES)

AFOSR/NA
875 North Randolph Street
Suite 325, Room 3112
Arlington VA 22203-1768

10. SPONSOR/MONITOR'S ACRONYM(S)

11. SPONSOR/MONITOR'S REPORT NUMBER(S)

12. DISTRIBUTION / AVAILABILITY STATEMENT

Approved for public release; distribution in unlimited.

13. SUPPLEMENTARY NOTES

14. ABSTRACT

The technique of Picosecond Time-Resolved Laser-Induced Fluorescence (PITLIF) was expanded to enable two-point hydroxyl (OH) series concentration time series measurements of turbulent jet flames. Measurements were obtained with two-point separation along the radial direction of the jet (Δr), i.e., the propagation direction of the horizontal laser beam, as well as axial two-point separations, i.e. along the axis of the jet, i.e., the z-direction. As the jet configuration is statistically axisymmetric, so that statistical analyses along the azimuthal direction can be considered insignificant, this allows complete coverage of the jet flame. Investigation of axial two-point statistics requires a different laser configuration than that of the previous radial two-point system: either a single vertical laser beam or two horizontal beams with adjustable vertical separation. The combustor used in this study has a closed base which does not permit vertical alignment of a laser; hence, the two-beam configuration was adopted. With the installation of our new diode-pumped laser system, which generates nearly ten times more UV power than before, the laser can now be split into two beams while still providing a sufficient signal level at each probe volume. This paper describes experimental details for this new approach and its demonstration within a well-studied turbulent hydrogen-nitrogen nonpremixed flame, the H3 flame (H_2/N_2 = 50:50, Re = 10,000).

15. SUBJECT TERMS
Turbulent Partially Premixed Flames, Autocorrelation Functions, Picosecond Time-Resolved Laser-Induced Fluorescence

16. SECURITY CLASSIFICATION OF:			17. LIMITATION OF ABSTRACT	18. NUMBER OF PAGES	19a. NAME OF RESPONSIBLE PERSON
a. REPORT	b. ABSTRACT	c. THIS PAGE			Dr. Julian M. Tishkoff
Unclassified	Unclassified	Unclassified	UL	24	19b. TELEPHONE NUMBER (include area code) (703) 696-8478

Standard Form 298 (Rev. 8-98)
Prescribed by ANSI

Two-Point Scalar Time-Series Measurements in Turbulent Partially Premixed Flames
AFOSR Grant FA95550-06-1-0064
Final Report

Prepared by

Galen B. King and Normand M. Laurendeau
School of Mechanical Engineering
Purdue University
West Lafayette, IN 47907-1288

February 2009

Abstract

The technique of Picosecond Time-Resolved Laser-Induced Fluorescence (PITLIF) was expanded to enable two-point hydroxyl (OH) concentration time series measurements of turbulent jet flames. Measurements were obtained with two-point separation along the radial direction of the jet (Δr), the propagation direction of the horizontal laser beam, and axial two-point separations along the jet axis. As the jet configuration was statistically axisymmetric, statistical analyses along the azimuthal direction could be considered insignificant, allowing complete coverage of the jet flame. Investigation of axial two-point statistics required a different laser configuration than that of the previous radial two-point system: either a single vertical laser beam or two horizontal beams with adjustable vertical separation. The combustor used in this study had a closed base that did not permit vertical alignment of a laser; hence, the two-beam configuration was adopted. With the installation of our new diode-pumped laser system, which generates nearly ten times more UV power than before, the laser could be split into two beams while still providing a sufficient signal level at each probe volume.

Table of Contents

Technical Discussion

Picosecond Time-Resolved Laser-Induced Fluorescence (PITLIF)

Quantitative measurements of radical species concentrations in flames are required for an understanding of important interactions between fluid mixing and chemical reactions [1]. Advances in laser-based techniques have made non-perturbing measurements of such species concentrations possible in recent years. In particular, laser-induced fluorescence (LIF) possesses both the spatial and temporal resolution necessary for monitoring radical concentrations in reacting flows (Barlow and Carter, 1994) [2]. Unfortunately, LIF usually suffers from an inverse dependence on the local quenching rate coefficient. Although laser-saturated fluorescence (LSF) permits measurements of species concentrations without recourse to quenching calculations, the LSF technique requires large input energies that demand a laser repetition rate on the order of 10 Hz. This repetition rate can provide mean concentrations and probability density functions (PDFs), but the 10 Hz repetition rate is clearly too slow to resolve species fluctuations in turbulent flames. High repetition rate lasers, on the other hand, can be utilized for measuring turbulent species fluctuations but the quenching rate coefficient must be obtained within sampling times on the order of the Kolmogorov time scale.

As a consequence of the above limitations for the usual LIF methods, the LIF protocol chosen for this research program utilized a mode-locked laser that had the temporal resolution and irradiance necessary to provide direct time-series measurements, thus yielding autocorrelation functions, as well as more traditional PDFs. The resulting optical technique, picosecond time-resolved laser-induced fluorescence (PITLIF), operated by monitoring the LIF signal using a novel four-bin integrated photon-counting procedure. Three sequential bins were used to resolve temporal decays rapidly to obtain fluorescence lifetimes at frequencies exceeding 10 kHz. The remaining bin was integrated over the entire fluorescence lifetime to obtain the integrated fluorescence signal. The quenching data from the first three bins ultimately could be used to correct the integrated data from the remaining bin, thus producing a temporal record of number density fluctuations that were independent of the local quenching environment. From this temporal record, quantitative autocorrelation functions and power spectral densities (PSD) could be determined corresponding to local concentrations in the flame. The resulting integral time scales then could be used for validation of theoretical turbulence and combustion models.

Over the past three years we implemented PITLIF for measurements of the OH integral time scale using a wide range of turbulent jet flames. From such data, suitable statistical information was compiled for comparisons to predictions from large-eddy simulations (LES). In addition, we developed a new version of PITLIF that permitted simultaneous time series at two nearby points in turbulent combustors. Before the two-point systems and results are presented in this report a review in some detail of the theory and basic photon-counting instrumentation for PITLIF is described.

Theory for PITLIF

The basic PITLIF procedure, which produces quenching-independent measurements of concentration, can be understood by applying the radiative rate equations to a simple two-level model. We begin with a laser pulse that excites molecules from the ground level to an excited electronic level. All of the initial population is assumed to be in the ground level before excitation; moreover, the width of the laser pulse, Δt, is short compared to the quenching time. For sufficiently low laser power, the number density in the excited level immediately following the laser pulse, N_2° (cm^{-3}), is given by

$$N_2^\circ = N_1^\circ \bar{W}_{12} \Delta t, \tag{1}$$

where N_1° is the initial number density of the species of interest and $\bar{W}_{12}$ is the average rate coefficient for stimulated absorption (s^{-1}), as computed from an integration over the exact laser pulse shape. Subsequent to the laser pulse, the population of the excited level decays back to the ground level. In the absence of laser irradiation, absorption and stimulated emission can be neglected so that during this decay the number density of the excited level is given by

$$N_2(t) = N_1^\circ \bar{W}_{12} \Delta t \exp(-t/\tau_{fl}), \tag{2}$$

where τ_{fl} is the excited-state (or fluorescence) lifetime (s). The excited-state lifetime is given in terms of the rate coefficient for spontaneous emission, A_{21}, and that for quenching, Q_{21}, by

$$\tau_{fl} = (A_{21} + Q_{21})^{-1}. \tag{3}$$

The temporal fluorescence signal depends linearly on both the number density in the excited level and the collection volume, V_c (cm^3). Hence, the temporally resolved fluorescence decay is given by

$$S(t) = \bar{W}_{12} \Delta t A_{21} V_c N_1^\circ \exp(-t/\tau_{fl}), \tag{4}$$

where *S(t)* represents the output of the PITLIF instrument in photons/second. While temporal analysis of *S(t)* yields the fluorescence lifetime, integration gives

$$S_F = \int_0^\infty S(t)\, dt = \bar{W}_{12} \Delta t A_{21} V_c \tau_{fl} N_1^\circ, \tag{5}$$

which corresponds to the integrated fluorescence signal. All of the terms in Eq. (5) can be determined through calibration except τ_{fl} and N_1°. For our two-level system, the excited-state lifetime can be determined from the decay represented by Eq. (4). Equation (5) then can be used to determine the initial number density corrected for electronic quenching. For a multilevel system, the total number density can be obtained from N_1° by using the appropriate Boltzmann fraction. In either case, the integrated fluorescence signal is proportional to the concentration of target molecules in the flame.

Previous PITLIF Measurements

We previously demonstrated that our photon-counting procedures for PITLIF can be used to monitor fluctuations in OH concentration on the time scale of turbulence [3-6]. During the last three years, we applied PITLIF to measurements of OH statistics in turbulent non-premixed and partially premixed flames [7, 8]. While making such measurements, we examined PITLIF statistics and LES simulations for OH in turbulent non-premixed flames. More recently, we

developed a two-point version of PITLIF that now permits, for the first time, determination of spatial, as well as temporal, statistics in turbulent flames [9, 10]. Further details of the experimental arrangements and salient results are reviewed in this and the following sections of this report.

Experimental Setup and Procedure

A diagram of the laser system, including the burner, is shown in Fig. 1. A Spectra Physics Tsunami, regeneratively mode-locked, Ti:Sapphire laser is pumped by a 20-W, Spectra Physics argon-ion, multi-mode laser and provides a pulse repetition rate of 80 MHz. For OH measurements, the resulting IR beam has a temporal pulse width of 2.0 ps and is frequency-tripled in a CSK SuperTripler. The output beam is re-collimated by two UV lenses and focused by a 20-cm focal length, 5.0-cm diameter UV lens to form the probe volume above the burner assembly. For the tripled beam, the spatial resolution is 200×200×40 μm^3 based on the beam diameter (e^{-2}) and the monochromator entrance slit width for the detection system. The laser power is 24-40 mW, which results in an average probe volume irradiance of ~2.5×10^7 mW/cm^2. The $R_1(11)$ transition of the (0,0) vibronic band (306.5 nm) of OH was chosen for excitation. This line displays an approximately ±5% Boltzmann fraction variation over the relevant temperature range of 1500-2500 K.

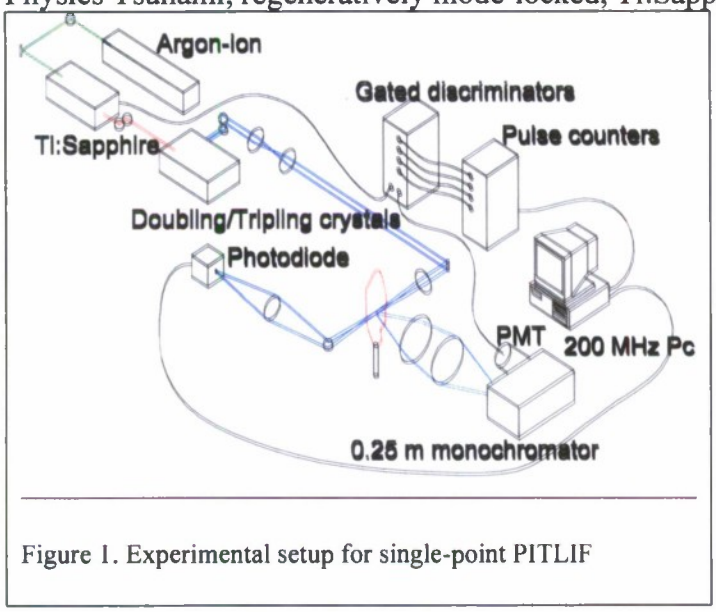

Figure 1. Experimental setup for single-point PITLIF

The OH fluorescence is collected at a 90-degree angle from the incident laser beam by using two 14.1-cm focal-length, 5.1-cm diameter UV lenses. The wavelength of the measured fluorescence is selected by use of a 0.25-m monochromator. An adjustable slit at the entrance to the monochromator limits the probe volume along the beam path. For most measurements, the

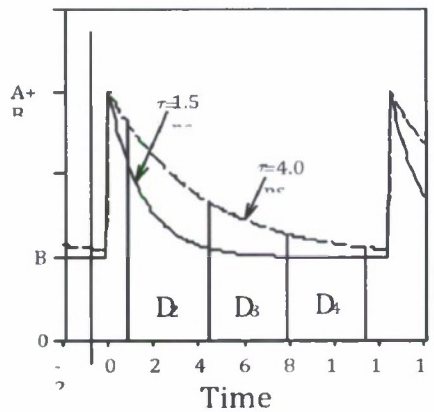

Figure 2. Graphical representation of the PITLIF method; D_2, D_3, and D_4 are each 3.5 ns wide. The background, *B*, is typical of flame emission, and the amplitude, *A*, is proportional to concentration.

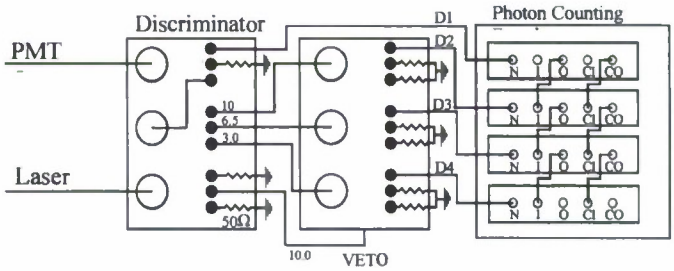

Figure 3. Wire schematic for the PITLIF system. N: NIM input from the discriminator; I: start signal input; O: start signal output; CI: channel advance input; CO: channel advance output. Unused signals are 50-Ω terminated, and 10.0, 6.5, and 3.0 represent the temporal delays (ns) placed in the respective lines.

spectral window was adjusted to give a total bandwidth of 10 nm centered at 309 nm. A Hamamatsu HS5321 photomultiplier tube (PMT) detected the fluorescence at the exit plane of the monochromator. This PMT had a risetime of 700 ps and a transit time spread of 160 ps. By biasing at −2450 V, the single-photon pulse height was enhanced for subsequent leading-edge discrimination. Figure 2 shows representative fluorescence decays with fluorescence lifetimes (τ_{fl}) of 1.5 and 4.0 ns, along with three areas, D_2, D_3, and D_4, specifying three of the four measurements for the gated photon counting system. The remaining measurement, D_1, which is not shown, is not gated and measures all photons; thus, D_1 represents the total integrated fluorescence under either curve in Fig. 2.

A detailed wire schematic for the gated, photon-counting system may be seem in Fig. 3. Briefly, this system consisted of two LeCroy Model 4608C, eight-channel discriminators connected to four EG&G Ortec logic-pulse counting boards. Several channels on the first discriminator were used to convert each PMT pulse into four logic (NIM) pulses. The second discriminator gated three of the four NIM pulses (D_2-D_4) from the first discriminator using a photodiode output from the Ti:Sapphire cavity. Separate cable delays for each of the three PMT inputs to the second discriminator ensured that each gate passed the appropriate portion of the fluorescence decay. The ungated PMT-NIM pulse from the first discriminator and the three outputs from the gated discriminator are counted separately by the four EG&G pulse counters shown schematically in Fig. 3. These comprised the measured bins D_2-D_4 of Fig. 2 and the integrated measurement D_1. The four photon-counting boards each had an 8192-channel memory and could be sampled simultaneously. Each channel acquired counts over many thousands of laser pulses as set in software. The maximum sampling rate (channel advance rate) for the boards is 500 kHz, well above that needed for turbulence studies.

The fluorescence lifetime, τ_{fl}, and the flame-emission background, B, can be found from the gated counts using the expressions (Pack et al., 1998) [11].

$$\tau_{fl} = \frac{\Delta t}{\ln[(D_2 - D_3)/(D_3 - D_4)]} \tag{6}$$

$$B = \frac{D_2 C^2 - D_4}{\Delta t (C^2 - 1)}, \tag{7}$$

where Δt was the width of each integrated bin (3.5 ns) and $C = \exp(-\Delta t/\tau_{fl})$. Following Eq. (4), the concentration of the excited state immediately following the laser pulse was proportional to the amplitude of the exponential decay, A, shown in Fig. 2, and could be determined from

$$A = \frac{D_2 - D_4}{\exp(-t_o/\tau_{fl})(1 - C^2)(1 - C)\tau_{fl}}, \tag{8}$$

where t_o was the delay between the laser pulse and the start of bin D_2. This amplitude was also directly proportional to the concentration of the ground state, following Eq. (1), which in turn was directly proportional to the total number density of the molecule of interest multiplied by a temperature-dependent Boltzmann fraction. Since the excitation wavelength could be chosen to minimize experimentally the variation of the Boltzmann fraction with temperature, A in Eq. (8) could be taken as proportional to the total number density.

Two-Point PITLIF

Radial Measurement System and Results

This two-point technique is capable of simultaneously monitoring OH time series at two locations, hence allowing the characterization of spatial structures in turbulent flames in addition to their temporal behavior. Several refinements have been made to improve upon the previous one-point instrument. Using a specially designed collection-lens system, off-axis optical aberrations have been minimized effectively in the probe volume. Furthermore, additional electronics have been installed which permit absolute species concentration measurements. As a preliminary study, two-point OH time-series measurements were taken in three standard turbulent non-premixed flames (H3, DLR_A and DLR_B) [12]. Two-point statistics, including space-time correlations, spatial autocorrelation functions and integral length scales were computed to elucidate the flame structure and turbulence-chemistry interactions.

Understanding complex physical and chemical processes in turbulent combustion requires temporally and spatially resolved measurement techniques. Non-premixed jet flames have been studied extensively because of their relative simplicity and well-defined flow field. Measurements of minor species concentrations in turbulent flames are important owing to their significance to chemical reactions and pollutant formation. Hydroxyl, in particular, is a good flame marker, whose fluctuations reveal important interactions between fluid mixing and chemical reactions.

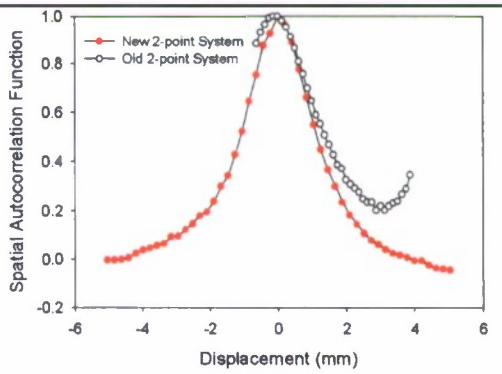

Fig. 4. Spatial autocorrelation function of H3 flame taken at the location of peak [OH] at x/D=20, using both the old and new two-point optical systems.

Time-series measurements of important scalars, such as temperature [13] and concentrations of OH [6] and CH [5], have been demonstrated using high repetition-rate, laser-based techniques. These measurements provide spectral characteristics and relevant time scales for scalars; however, as pointwise measurements, they give no information on spatial structures. To circumvent this limitation, simultaneous multipoint or even 1D or 2D time-series measurements are required. Examples of this endeavor include multipoint OH chemiluminescence measurements [14], two-point temperature measurements [15], and high repetition-rate planar laser-induced fluorescence (PLIF) [16]. For minor species, two-point PITLIF was previously developed, which provided quantitative concentration measurements of radical species at relevant turbulent temporal and spatial scales [10, 11].

Modifications have been made to improve the earlier version of the two-point PITLIF system. Optical aberrations were found to have significant effects on our previous two-point statistics [9]. In particular, aberrations occurred when either probe volume deviated from the optical axis of the detection system. Furthermore, at large displacement distances, partial overlap arose between images of the two probe volumes. This overlap created artificial

coherence between signals from the two probe volumes, which was exhibited as a secondary peak in the spatial autocorrelation function, as depicted in Fig. 4.

To address this problem, we designed a new lens system via ZEMAX software, which now produces an aberration-limited blur spot of less than 130 μm at object positions up to 6 mm away from the optical axis. As shown in Fig. 5, the current optical system is composed of one custom-made aspherical lens (L1), a 10-cm diameter UV beamsplitter (BS), and two pairs of plano-convex and meniscus lenses (L2 and L3; L4 and L5). The new setup has a magnification ratio of 1.19 and a working f# of 2.8. Each probe volume is 485×485×210 μm^3, which is determined by the diameter of the laser beam and the entrance slit width of the monochromators. PITLIF utilizes the principle of triple-bin integration [10] which can correct for the effect of electronic quenching on-the-fly. The insertion of four additional multichannel scalers allows for absolute species concentration measurements at both probe volumes.

To demonstrate the effectiveness of this revised setup, two-point PITLIF data were taken at the same position (peak [OH] at x/D=20) within the same flame used by Zhang et al [9]. The derived spatial autocorrelation function shown in Fig.4 displays an approximately exponential decay without a secondary peak, as expected from the typical statistics of a turbulent field.

For this study, three non-premixed flames (H3, DLR_A and DLR_B) were investigated chosen from the Turbulent Nonpremixed Flames (TNF) Workshop. Two-point OH measurements were taken at locations corresponding to the mean peak [OH] as well as positions along the jet centerline, with x/D ranging from 10.00 to 53.25, where x/D=35 and x/D=53.25 correspond to the respective flame tips of the H3 and DLR_A flames. The mean OH concentrations were compared with the available data from the TNF database [12] (the detailed comparison can be found in Zhang et al [10]). The measurements agree quite closely except at two locations: the jet centerline at x/D=50 in DLR_A and peak [OH] at x/D=20 in DLR_B. This discrepancy likely is due to deviations in position between the two measurements and increased uncertainty at the jet centerline owing to the small signal-to-background ratio.

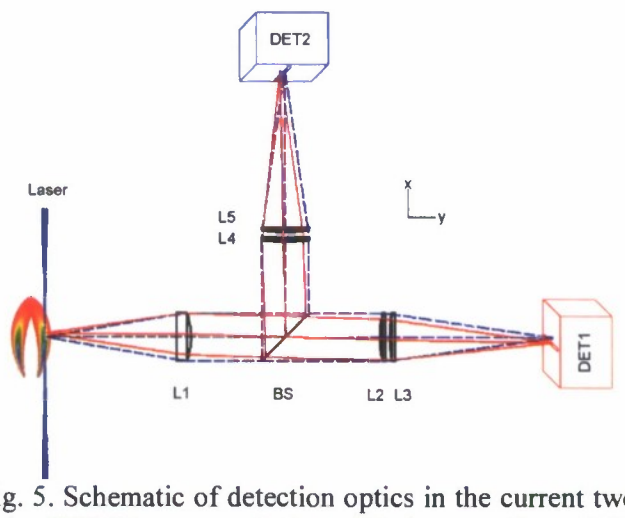

Fig. 5. Schematic of detection optics in the current two-point PITLIF system. L, lens; BS, beam splitter; DET, detector assembly consisting of a monochromator and photomultiplier tube. Solid and dashed rays identify the signal from two different probe volumes.

Given two simultaneous [OH] time series, a number of two-point statistics can be evaluated, including the space-time correlation, spatial autocorrelation function, and integral length scale. The normalized space-time correlation is defined as [11],

$$f_{st}(\Delta r,\Delta t)=\frac{\left\langle OH'(r,t)OH'(r+\Delta r,t+\Delta t)\right\rangle}{\left[\left\langle OH'(r,t)^2\right\rangle\left\langle OH'(r+\Delta r,t+\Delta t)^2\right\rangle\right]^{1/2}}, \quad (9)$$

where $OH'(r,t)$ is the fluctuating component of hydroxyl concentration at radial location r and time t, while Δr and Δt are the displacement between the two probe volumes and the lag time, respectively. Figure 6 displays the calculated space-time correlation at two peak [OH] locations in the H3 flame. Positions near the flame tip show a broader peak along the displacement axis, indicating a larger coherence region.

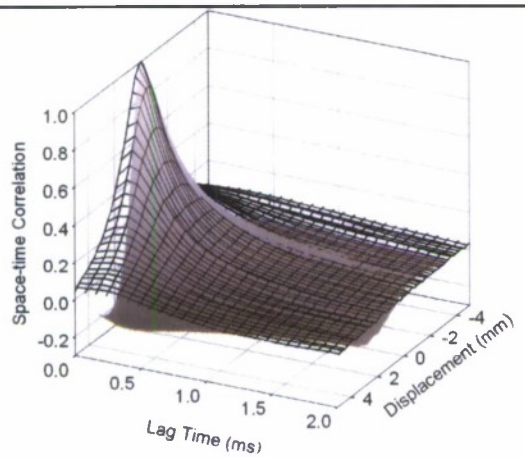

Fig. 6. Space-time correlation at two peak [OH] locations in the H3 flame: (a) x/D=10 (shaded surface); (b) x/D=30 (mesh).

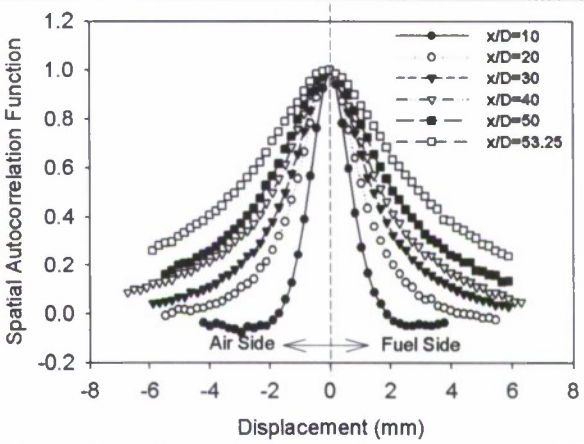

Fig. 7. Normalized spatial autocorrelation functions for the DLR_A flame: (a) at peak [OH] locations.

The normalized spatial autocorrelation function is related to the space-time correlation by

$$f_s(\Delta r) = f_{st}(\Delta r, \Delta t = 0). \tag{10}$$

Figure 7 displays spatial autocorrelation functions for the DLR_A flame at peak [OH] locations. The full-width-at-half-maximum (FWHM) of the curve becomes greater farther downstream, which is a manifestation of the broadening coherence region mentioned earlier. In general, the spatial autocorrelation function is symmetric between the air and fuel sides. Exceptions occur primarily near the nozzle (x/D ≤ 10). This abnormality might be explained by the evolution of

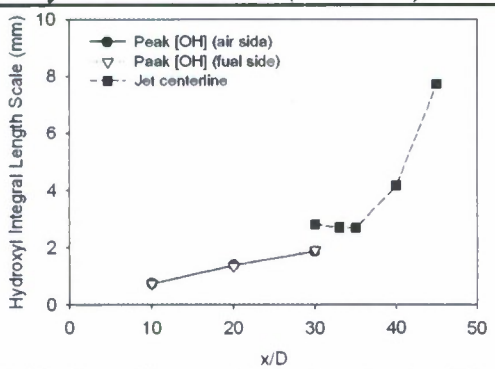

Fig. 8. Hydroxyl integral length scales for H3 flame.

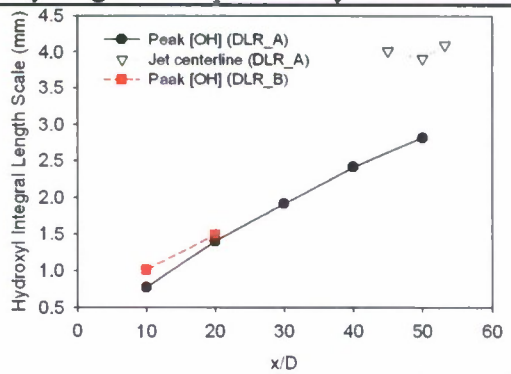

Fig. 9. Hydroxyl integral length scales for DLR_A and DLR_B flames.

flame structures. In turbulent jet diffusion flames, the reaction zone lower in the flame (e.g. x/D≤5 for the DLR_A flame) is composed of thin layers located outside the turbulent fuel jet [18]. Because of relaminarization, the reaction zone essentially acts as a shield blocking the

penetration of fuel vortices; hence, the reaction zone and air side remain laminar. Farther downstream, the flame front becomes more wrinkled as the effect of laminarization diminishes; therefore, the asymmetry of the spatial autocorrelation function at x/D=10 probably is due to residual laminarization.

The OH integral length scale can be determined by integrating the spatial autocorrelation function over its displacement, Δr, so that

$$l_I = \int f_s(\Delta r) d\Delta r . \tag{11}$$

While the spatial autocorrelation function exhibits asymmetry near the nozzle, the calculated integral length scales are about the same on both sides (Fig. 8). The hydroxyl length scales are well resolved and increase linearly with axial distance at peak [OH] locations (Figs. 8 and 9), consistent with observations of integral length scales for mixture fraction at mean stoichiometric radii in methane/air jet diffusion flames [19]. This result suggests that OH fluctuations at peak [OH] locations essentially are dominated by flame motions, a confirmation of flamelet theory. The integral length scales basically are constant along the jet centerline below the flame tip and increase rapidly above the flame tip.

Axial Measurement System and Results

The previously reported two-point OH time series for turbulent jet flames were obtained with two-point separation along the radial direction of the jet (Δr), i.e., the propagation direction of the horizontal laser beam. For a thorough understanding of OH fluctuations, we also desire two-point statistics using separations along other directions. As the jet configuration is statistically axisymmetric so that statistical analyses along the azimuthal direction can be considered insignificant, the only remaining direction of interest is along the axis of the jet, i.e., the z-direction. Investigation of axial two-point statistics requires a different laser configuration than that of the previous radial two-point system: either a single vertical laser beam or two horizontal beams with adjustable vertical separation. The combustor used in this study has a closed base that does not permit vertical alignment of a laser; hence, the two-beam configuration has been adopted. With the installation of our new diode-pumped laser system, which generates nearly ten times more UV power than before, the laser now can be split into two beams while still providing a sufficient signal level at each probe volume. This section describes experimental details for this new approach and its demonstration within a well-studied turbulent hydrogen-nitrogen nonpremixed flame, the H3 flame (H_2/N_2 = 50:50, Re = 10,000).

For this variation on the PITLIF technique, the mode-lock Ti: Sapphire laser is pumped by a 532-nm diode-pumped cw laser at 13.5 W. The generated IR pulsed beam at a repetition rate of 80 MHz then is frequency-tripled into the UV. The output UV laser pulse has a temporal width of 2 ps and a spectral width of 0.3 nm. Its wavelength is tuned to 306.5 nm to excite multiple transitions in the ($v' = 0$, $v'' = 0$) vibrational band of the $A\ ^2\Sigma^+ - X\ ^2\Pi_i$ electronic system of OH selectively. The excitation wavelength is selected to minimize the temperature dependence of the overall Boltzmann fraction, so that quenching-corrected fluorescence signals can be converted directly to OH concentrations. Simulations of the OH absorption spectrum versus temperature, using the spectroscopic code developed by Seitzman [20], verify a variation in absorption coefficient of only ±5% at 1500-2500 K.

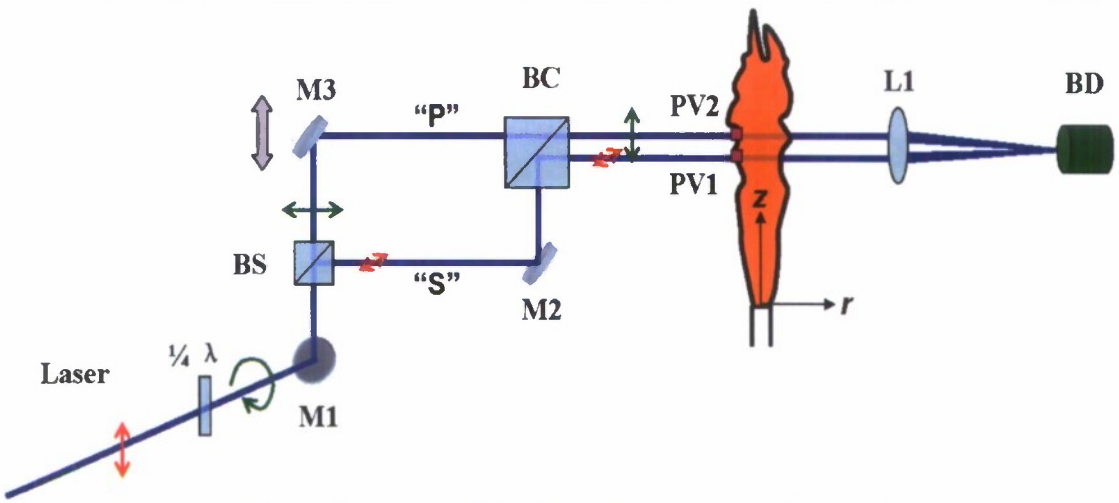

Figure 10. Schematic of the laser alignment used for the current two-point PITLIF system: ¼ λ, zero-order quarter waveplate; M, mirror; BS, polarizing cube beamsplitter; BC, polarizing cube beam combiner; PV, probe volume; L, lens; BD, beam dump. The red and green arrows identify the polarization. "P" and "S" designate two split laser beams based on their polarizations.

Figure 10 shows the experimental layout used for aligning the two beams of this investigation. The linearly polarized UV beam from the laser system first is converted into a circularly polarized beam with a zero-order quarter waveplate (¼ λ) and then split into two beams ("P" and "S") with different polarizations within a polarizing beamsplitter (BS). The two split beams subsequently are folded with mirrors (M2 and M3) and recombined with a beam combiner (BC) to form two parallel horizontal beams across the flame. The axial two-point separation then can be adjusted continuously by translating the M3 mirror. To ensure day-to-day consistency in performance, all these optical components except the wave-plate and lens are mounted on a 30 cm × 30 cm vertically placed optical breadboard. This arrangement of two horizontal laser beams offers much freedom for two-point measurements, as the separation between the two probe volumes (PV) can be made radial, axial, or both.

The optical detection system and the subsequent photon-counting system are essentially the same as those used in previous radial two-point experiments [21]. To summarize, fluorescence photons from two probe volumes are collected by an aspherical lens, split by a beamsplitter, and eventually focused by lens doublets onto corresponding detector assemblies, with each consisting of a monochromator and PMT. Adjustment of two-point separation is achieved by translating one detector while keeping the other one fixed. As the entrance slit of each monochromator defines the location of the corresponding probe volume, calibration is required to establish the ratio between translation of the probe volume and that of the detector by imaging a needle tip placed at the probe volume. For both the radial and axial directions, this ratio is found to be 1.19, which matches the magnification ratio of the collection lens system. Each probe volume has dimensions of 350×350×210 μm^3, as defined by the laser-beam diameter (e^{-2}) and the entrance-slit width of the monochromator.

A new problem that emerges for axial two-point measurements is interference between the two laser beams. The p- and s- polarized beams have a vertical dimension of 330 and 190 μm at the focal point, respectively, which implies full or partial overlap between the two beams for Δz ranging between –260 and 260 μm; moreover, the height of the entrance slits for the

monochromators was set at approximately 750 μm, corresponding via magnification effects to 625 μm of vertical acceptance window at the probe volumes. This fact suggests that it is still possible to collect fluorescence photons from both laser beams, even though the two beams are well separated. To avoid all interference from the two beams, the minimum two-point separation $|\Delta z|$ should be around 475 μm. Experimentally, the two-beam interfering range for Δz can be determined by examining the change in signal detected by the fixed PMT versus two-point separation. This interference range can be defined as that beyond which the photon rate has minimal variation. For all measurements, the interference range was found to be between –1.0 and 0.5 mm; hence, measurements within this Δz range were rejected. For the systems studied so far, this minimum separation has little effect on our ability to resolve coherent structures within turbulent flames.

Space-time correlations derived from the axial two-point time-series measurements are shown in Fig. 11 for z/D = 10. At zero two-point separation ($\Delta z = 0$), the space-time correlation reduces to the temporal autocorrelation function, from which we may determine the integral time scale. This measurement thus provides an independent way of measuring this macroscale, which is found to match within 10% the results from previous single-point and radial two-point measurements [22]. Compared with the previously reported radial space-time correlations, the

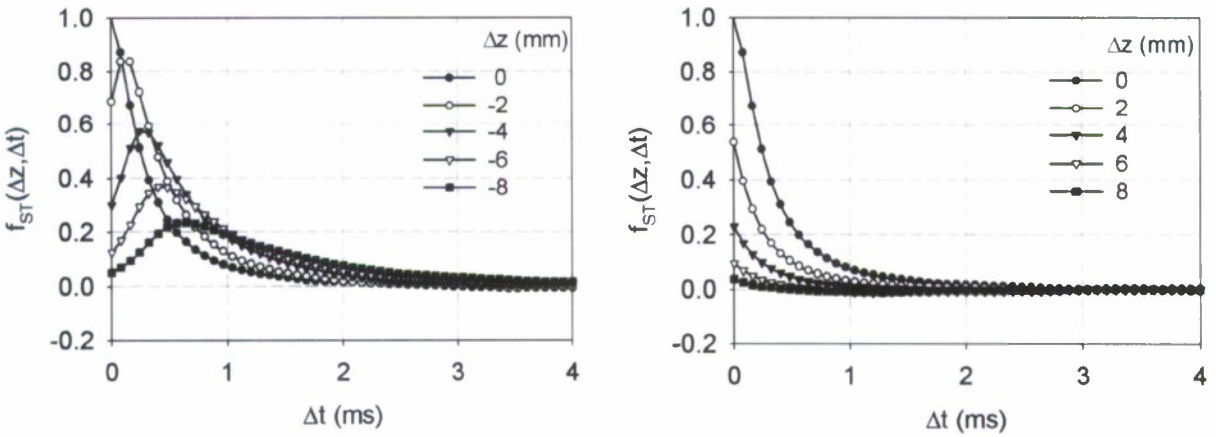

Figure 11. Space-time correlations of [OH] fluctuations for two-point separations along the axial direction at the radial peak [OH] location corresponding to z/D = 10. Negative Δz corresponds to the upstream direction and vice versa.

axial space-time correlations have some peculiar features. First, for nonzero two-point separations at upstream locations, i.e., when the second probe volume is moved upstream, each correlation curve has its maximum at a certain time delay. This feature appears because OH structures are convected from upstream locations and take this amount of time to reach the fixed probe volume. Hence, the time delay is equal to the two-point separation divided by the convection velocity. Second, a progressive decrease below unity occurs in the correlation maxima with increasing two-point separation. The reason for this behavior is that during the convection process, the OH structures experience chemical reactions and turbulent mixing, so that the longer the time it takes to reach the fixed probe volume, the less the structures look like the original ones. A similar phenomenon has been observed for space-time correlations of velocity in a nonreacting jet (Wills) [23] and for those of temperature in premixed jet flames (Ghenai and Gökalp) [24].

Convection of turbulence and scalar structures stems from Taylor's original hypothesis on grid turbulence. According to Taylor [25], at low turbulence levels the spatial pattern of fluctuating velocity is rigidly translated to other locations at the mean-flow velocity; hence,

$$f_{ST}\left(\Delta z - V_C \tau_1, \Delta t\right) = f_{ST}\left(\Delta z, \Delta t + \tau_1\right), \quad (12)$$

where V_C is the convection velocity. This hypothesis, the so-called frozen-turbulence approximation, is accurate only for grid turbulence and typically is not strictly valid for free shear flows, such as jets (Pope) [26]. Space-time correlations measured in this investigation confirm that gradual distortion occurs for OH structures when being convected downstream within the jet.

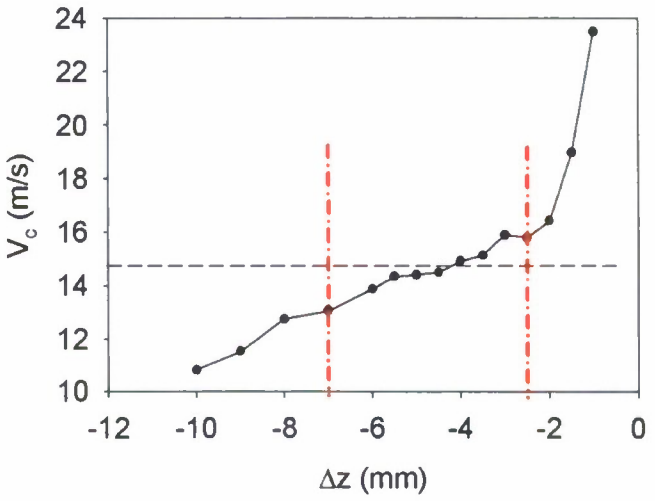

Figure 12. Convection velocity of OH structures estimated from space-time correlations of various two-point separation distances at the radial peak [OH] location for z/D = 10. The effective convection velocity is defined as the average (the dashed line) after discarding the first and last three points owing to errors from truncation and curve-fitting.

Even though Taylor's hypothesis is not strictly correct, convection of turbulent eddies and accompanying scalar structures at steady velocity is a prevalent concept. The convection velocity, which may not be necessarily the mean-flow velocity, then can be defined as the two-point separation divided by the time delay corresponding to the correlation maximum,

$$V_C = \frac{\Delta z}{\tau_d}, \quad (13)$$

where the delay time τ_d can be described mathematically as

$$\partial f_{ST}\left(\Delta z, \Delta t\right) / \partial\left(\Delta t\right)\Big|_{\Delta t = \tau_d} = 0. \quad (14)$$

A cubic spline curve can be used to fit the correlation curve $f_{ST}(\Delta z, \Delta t)$ to find the delay time, τ_d, through Eq. (12). The calculated convection velocity at the radial peak [OH] location for z/D = 10 is shown in Fig. 12. Clearly, the convection velocity is not a single value, and instead depends somewhat on the choice of two-point separation. This ambiguity in convection velocity has been noted previously for velocity measurements in non-reacting jets [23]; variable choices were proposed for this velocity that, however, do not shed more light on the underlying physics. For this investigation, an effective convection velocity is determined as the average of convection velocities at different two-point separations. Points are discarded at small and large separations, as such calculations are likely contaminated owing to truncation errors at small separations and errors resulting from curve-fitting at large separations. We note that other ways are available for calculating the convection velocity, either by the constant time-delay method [23] or based on cross-spectra [27], which may offer greater significance for acoustic noise generation.

The space-time correlation for downstream two-point separations in Fig. 12 is quite different from that for upstream separations. The maximum of each correlation curve occurs at zero delay time, and undergoes faster decay with respect to increasing two-point separation. The reason for this behavior is that downstream structures cannot travel back and thus are unable to relate better to the fixed probe volume for $\Delta t > 0$. This feature illustrates that the space-time correlation for a stationary process is typically not symmetric with spatial separation; rather,

$$f_{ST}(\Delta z, \Delta t) = f_{ST}(-\Delta z, -\Delta t) \neq f_{ST}(-\Delta z, \Delta t), \quad (15)$$

which can be shown easily by switching the roles of the two probe volumes. The different features of axial space-time correlations between positive and negative separations also should be observed for radial space-time correlations at non-zero radial positions; however, owing to the much smaller radial velocity for axisymmetric jets, the radial convection of scalar structures is much less prominent, which may explain the failure to observe such convection for the thermal structures of (Ghenai and Gökalp) [24] .

A different way of studying the space-time correlation is to develop a constant correlation map. For an ideal Taylor's model, constant space-time correlations satisfying Eq. (9) would be shown in the (Δz, Δt)-plane as parallel lines with a slope equal to the convection velocity, $-V_C$, indicating rigid convection of scalar structures at a constant mean velocity. As shown in Fig. 13, space-time correlation maps of OH concentration retain some features of Taylor's model. The constant correlation lines are approximately parallel to each other over a narrow range of two-point separations; however, they eventually form close loops over the large, negative Δz region, further confirming the idea of non-rigid convection of scalar structures within jets. Furthermore, the variable slopes of the constant correlation lines make the definition of an unambiguous convection velocity impossible; instead, the convective velocity becomes a function of spatial separation, as indicated by Fig. 13. Compared with the radial peak [OH] location at z/D = 10, the space-time correlations at the jet axis for z/D = 45 offer greater resemblance to an ideal Taylor's model. A survey over all measurements of this study further suggests that space-time

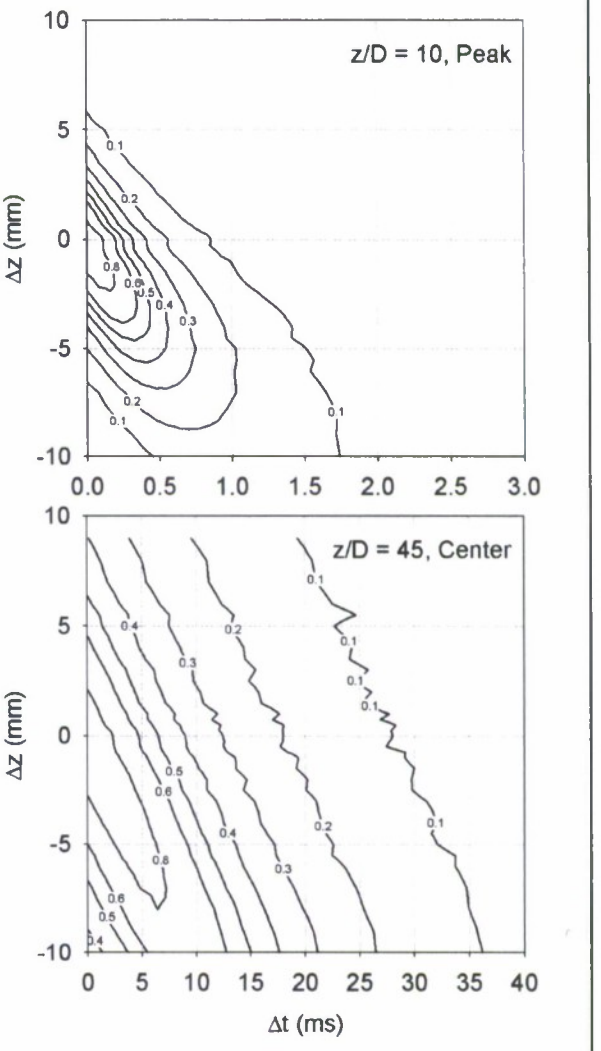

Figure 13. Space-time correlation maps of OH concentration fluctuations for two-point separations along the axial direction at radial peak [OH] for z/D = 10 and at the jet axis for z/D = 45. Negative Δz corresponds to the upstream direction.

correlations at the jet axis and at higher z/D more closely approach Taylor's ideal case than those off the centerline and at lower z/D. This phenomenon is quite strange, as axial positions at high z/D have higher turbulence levels so that Taylor's hypothesis should be more likely to fail.

Conclusions and Recommendations

A two-point high-speed laser-induced fluorescence technique (PITLIF) for simultaneously capturing fluctuations of minor species at two spatial locations has been developed. Various issues in instrumentation for two-point PITLIF have been presented and applications of this technique have been demonstrated for measurements of OH in a variety of turbulent nonpremixed and partially premixed jet flames.

Conclusions

The following conclusions can be made from this investigation.

(1) Simultaneous two-point quenching-corrected measurements have been made for the first time at sampling rates reaching 40 kHz. This system offers sufficient spatial and temporal resolution for investigating two-point statistics of minor species concentrations, including the space-time correlation, spatial autocorrelation and integral length scale. In principle, this technique can be applied to a variety of minor species, including OH, CH, and NO, provided that enough laser power can be obtained at the excitation wavelength of the molecule of interest.

(2) Optical aberrations of the optical detection system are important for both single-point and two-point measurement techniques. Such aberrations have a significant impact on spatial resolution and the measured two-point statistics; hence, meticulous optical design should be performed to minimize optical aberrations.

(3) For all flames of this investigation, fluctuations in fluorescence lifetime have a negligible effect on the derived two-point statistics. Hence, two-point statistics calculated from fluorescence bin counts can be treated as concentration; therefore, uncertainties involved in the quenching correction process can be avoided and high sampling rates can be achieved, which provides the potential for studying flames at high Reynolds numbers.

(4) For turbulent nonpremixed jet flames, the temporal autocorrelation functions exhibit universal self-similarity, while the radially spatial autocorrelation functions are self-similar for small to medium two-point separations, owing to the non-universality of large-scale fluctuations that suggests the hydroxyl integral time scale is sufficient for characterizing macroscale temporal fluctuations; however, the integral length scale may be meaningful only to a certain spatial extent, for instance, within the corrugation scale of the OH structures. The existence of coherent vortices near the flame base is found to be responsible for negative spatial correlations, which become less appreciable with increasing jet Reynolds number.

(5) For turbulent nonpremixed jet flames, the radial hydroxyl integral length scale displays different trends at mean radial [OH] peaks and close to the flame tip. At mean radial [OH] peaks, the OH integral length scale is related to corrugation of the OH layer and is dictated by the average eddy size, thus following a linear relation with axial distance. Around the flame tip, the OH integral scale is close to that of a conserved scalar and of the dynamic scale. Below the flame tip, the OH integral length varies little with

increasing z/D owing to the effect of enhanced dissipation of large-scale vortices at increasingly high temperatures. Beyond the flame tip, the OH length scale increases more than linearly with z/D because of penetration of large-scale buoyancy-induced vortices. The radial integral length scale depends weakly on the jet Reynolds number but strongly on fuel dilution owing to its influence on flame length and overall flame structures.

(6) Hydroxyl integral time scales in turbulent nonpremixed jet flames can be scaled reasonably by the ratio of OH integral length scale and the primary velocity component along the same direction. The integral time scale depends strongly on both the jet Reynolds number and fuel dilution. For the flames under investigation, OH integral time scales can be related approximately linearly to the mean flame-front passing period at most locations within flames, suggesting that the integral length scale indicates the mobility of the flame front.

(7) For turbulent partially premixed jet flames, temporal and radially spatial autocorrelation functions are generally not self-similar, suggesting that the OH integral time and radial length scales cannot be treated as parameters characterizing solely macroscale fluctuations of [OH] in these flames. At sufficient premixing levels, the flames exhibit a double-flame structure, where the premixed front displays more rapid [OH] fluctuations than the nonpremixed front. The spatial autocorrelation function displays strong negative values, including at far downstream locations, suggesting the existence of a prolonged region of coherent vortices and laminarization, which may result from the thick high-temperature region between the two flame fronts.

(8) For turbulent partially premixed jet flames, temporal fluctuations of [OH] at the premixed flame front are characterized by both a fast time scale corresponding to fast flamelet crossings and a slow time scale, which is approximately ten times smaller than the fast scale. At the nonpremixed front, the integral time scale follows a scaling relation similar to that for purely nonpremixed jet flames.

(9) For turbulent partially premixed jet flame, the radial integral length scale at the premixed flame front is greater than that at the nonpremixed flame front for the same axial distance. At the nonpremixed front, the radial integral length scale varies in a nonlinear fashion with respect to axial distance, which may be related to the prolonged laminarized region.

(10) Axial two-point OH statistics for nonpremixed flame exhibit prominent features of OH convection. Convection of OH structures occurs at approximately the flow velocity and deviates from Taylor's hypothesis with distortion of OH structures. The axial length scale is generally greater than the radial length scale, again suggesting elongated OH structures, which become isotropic at far downstream locations. This integral length scale does not follow the dynamic length scale, as measured in turbulent nonreacting jet, which suggests the influence of heat release and localization of OH structures.

In general, OH chemistry does not seem to have an appreciable effect on macroscale statistics, including space-time correlations and integral time and length scales.; however, such chemistry may contribute to high-frequency components of OH PSDs, leading to the absence of a power-law region, as would be expected for a scalar in a turbulent system.

A method for studying the statistics of flame front motion has been devised, by threshold-filtering the OH concentration. A comparison between flame-front and OH statistics shows that these two statistics are comparable over most measurement locations. However, deviations occur near the flame tip, where OH structures are typically thick.

An ambiguous definition of the flame front in this region is challenging, as the combustion zone is typically thin throughout a flame [18]. The validity of this analysis is subjected to further scrutiny.

The distinction between partially premixed and nonpremixed jet flames is interesting. A prolonged laminarized region resulting from the high temperature between the two flame fronts is proposed as responsible for the peculiar spatio-temporal statistics of partially premixed flames. Possible crossing of the premixed front at the mean nonpremixed peak may result in the measured bimodal PDF in OH concentration. Other issues also require further clarification, such as the slow time scale of OH fluctuations at the premixed front and the cause of the visible flame-tip pulsation.

Recommendations

Based on the progress to date, the following recommendations can be given.

(1) The current two-point PITLIF setup can be improved further by installing separate detection optics for the two different detectors, with the detection optics and detector corresponding to the movable probe volume mounted on a single translation stage. This approach offers two advantages. First, it avoids off-axis optical aberrations, as the movable probe volume is always on the optical axis. Second, it avoids splitting of the fluorescence signal with a beamsplitter, thus doubling the detected signal level. In addition, the laser system, including the Tsunami laser and the harmonic generator, may be put in an enclosure with local climate control. The ensuing advantage is avoidance of dramatic fluctuations in temperature and humidity, which are typical when running a flame. This tactic is quite critical for ensuring stable laser operation.

(2) Though a powerful technique, two-point PITLIF is a single-scalar measurement, which cannot reveal a full picture of turbulent flames. As processes in turbulent combustion are highly correlated in a nonlinear fashion, it is quite desirable to make multi-scalar measurements. With the current facility, it is possible to perform simultaneous OH and temperature measurements, as temperature can be measured by an available argon-ion laser. With simultaneous [OH] and T, the effects of scalar dissipation rate can be investigated for both scalars in turbulent nonpremixed flames, which is valuable for turbulent combustion modeling. As T can be related solely to mixture fraction in a fuel-lean or fuel rich condition, we also may use two-point [OH] measurements to define the stoichiometric condition by tracking the movement of the flame front. The simultaneous T time series may be converted to a mixture fraction time series, which provides more significance than a species time series. Additionally, the simultaneous [OH] and T data definitely will shed more light on less understood turbulent partially premixed flames.

(3) The current technique may be extended to applications involving CH or NO. For NO, the quadrupled output of the harmonic generator can be used (~226 nm). By doping the flow with NO, NO concentration can be used as a surrogate for studying mixing processes within turbulent nonreacting flows or even flames for which NO production and destruction are less significant as compared to any dopant concentration. For CH, the doubled output of the harmonic generator can be used (~431 nm). As CH is a better marker of the flame front than OH [18], its time series may provide better pictures of turbulence-flame interactions.

(4) Time and space series (TASS) simulations can be adopted to extend the use of two-point OH time-series measurements in turbulent nonpremixed jet flames. With this method,

realistic mixture fraction time series can be simulated, along with integral time and length scales of mixture fraction.

Finally, with two-point PITLIF producing rich information on OH fluctuations, it is desirable to collaborate with combustion modelers to make use of these data to validate advanced combustion models.

Personnel

Professors Galen B. King, Normand M. Laurendeau, and Michael W. Renfro are co-principal investigators for this research program. Mr. Andrew Noble and Mr. Keian Kirkegaard are Ph.D. students working on the project at Purdue University. Dr. Jiayao Zhang worked on the project until he received his Ph. D. from Purdue University in December (2007) and is currently a Post Doctoral Researcher at Sandia National Laboratory. Ms. Kristin Kopp-Vaughan and Mr. Stanislav Kostka are MS students working on this project at the University of Connecticut. Mr. Noble, Mr. Kirkegaard, Mr. Kostka, and Ms. Kopp-Vaughn are United States Citizens.

Honors /Awards

Professor Laurendeau is a fellow of both the American Society of Mechanical Engineering and the Optical Society of America. Professors King and Renfro are members of American Society of Mechanical Engineering, Optical Society of America, and the Combustion Institute. Professor Renfro was promoted from Assistant to Associate Professor this year at the University of Connecticut.

Publications:

1. Zhang, J., Venkatesan, K.K., King, G.B., and Laurendeau, N.M., "Two-Point Time-Series Measurements of Minor-Species Concentrations in a Turbulent Nonpremixed Flame," *Optics Letters*, Vol. 30, No. 23, 3144-3146, 2005.

2. Guttenfelder, W.A., Renfro, M.W., Laurendeau, N.M., Ji, J., King G.B., and Gore, J.P., "Hydroxyl Time Series and Recirculation in Turbulent Nonpremixed Swirling Flames," *Combustion and Flames,* 147, 11-21, 2006.

3. Zhang, J., King, G. B., Laurendeau, N.M., and Renfro, M.W., "Two-point time-series measurements of hydroxyl concentration in a turbulent nonpremixed flame," Applied Optics, Vol. 46, No. 23, May, 2007.

4. Meyers, T. R., King, G. B., Gluesenkamp, M., and Gord, J. R., "Simultaneous high-speed measurements of temperature and lifetime-corrected OH laser-induced fluorescence in unsteady flames," Optics Letters, Vol. 32, No. 15, August 1, 2007.

5. Venkatesan, K. K., Zhang, J., King, G. B., Laurendeau, N. M., and Refro, M. W., "Hydroxyl space-time correlation measurements in partially premixed turbulent opposed-jet flames," Appl. Phys. B 89, 129-140, 2007.

6. Zhang, J., King, G.B., Laurendeau, N.M., and Renfro, M. W., "Two-point OH time-series statistics for turbulent partially premixed jet flames," Paper # B21, 5th US Combustion Meeting, Organized by the Western States Section of the Combustion Institute, University of California, San Diego, March 25-28, 2007.

7. Gluesenkamp, M. W., Vendatesan, K. K., Noble, A. C., King, G. B., Laurendeau, N. M., Kopp-Vaughn, K. M., and Renfro, M. W., "Simultaneous Hydroxyl and Pressure Time-Series Measurements in A Self-Excited Acoustically-Driven Tube Combustor." Central States Section 2008 Technical Meeting, The Combustion Institute, University of Alabama, Tuscaloosa, Al., April 20-22, 2008, paper A1-2.

8. Kopp-Vaughn, K.M., Renfro, M. W., and King, G. B., "Flame Structure Measurements and Principal Component Analysis in Self-Excited Acoustically-Driven Premixed Flames." Central States Section 2008 Technical Meeting, The Combustion Institute, University of Alabama, Tuscaloosa, Al., April 20-22, 2008, paper A3-4.

Theses:

1. "Design and Analysis of a Thermoacoustically Unstable Tube Combustor," Matthew Michael Gluesenkamp, MSME Purdue University, December 2007.

2. "Development of a Two-Point High-Speed Laser-Induced Fluorescence Technique and its Appkications to Turbulent Jet Flames for OH Concentration," Jiayao Zhang, Ph. D. Purdue University, December 2007.

3. "Hydroxyl Spatio-Temporal Statistics for Turbulent Partially Premixed Opposed-Jet Flames," Krishna Kumar Venkatesan, Ph. D. Purdue University, May 2007.

Interactions /Transitions

Our research group has continued its commitment to working and maintaining strong interactions with personal at the Air Force Research Laboratories (AFRL). Our point of contact was Dr. James R. Gord, AFRL/RZTC Wright-Patterson Air Force Base, Ohio. Professor King and MSME student Matthew Gluesenkamp spent 12 weeks at AFRL during the summer of 2006. Professor King spent 12 weeks at AFRL during the summer of 2007. Professor King and Ph. D. student Andrew Noble spent 12 weeks at AFRL during the summer of 2008. Professor King was supported by the Summer Faculty Fellowship Program of the American Society of Engineering Education during these three summers. One collaborative paper from this interaction has been published and other manuscripts are in various stages of development at this time. Additionally, a two-point PITLIF optical system similar to the one developed at Purdue and described in this report was constructed at AFRL. Several additional papers are either in review or other stages of being written as a result of this interaction.

References:

1. Drake, M.C., Pitz, R.W., Lapp, M., Fenimore, C.P., Lucht, R.P., Sweeney, D.W., and Laurendeau, N.M., 1984, "Measurements of superequilibrium hydroxyl concentrations in turbulent nonpremixed flames using saturated fluorescence," *Twentieth Symposium (International) on Combustion*, The Combustion Institute, Pittsburgh, pp. 327-335.

2. Barlow, R.S., and Carter, C.D., 1994, "Raman/Rayleigh/LIF measurements of nitric oxide formation in turbulent hydrogen jet flame," *Combustion and Flame*, Vol. 97, pp. 261-280.

3. Renfro, M.W., Pack, S.D., and Laurendeau, N.M., 1999, "A pulse-pileup correction procedure for rapid measurements of hydroxyl concentrations using picosecond time-resolved laser - induced fluorescence," *Applied Physics B*, Vol. 69, pp.137-146.

4. Renfro, M.W., King, G.B., and Laurendeau, N.M., 1999, "Quantitative hydroxyl concentration time-series measurements in turbulent nonpremixed flames," *Applied Optics*, Vol. 38, pp. 4596-4608.

5. Renfro, M.W., King, G.B., Laurendeau, N.M., 2000, "Scalar time-series measurements in turbulent $CH_4/H_2/N_2$ nonpremixed flames: CH.," *Combustion and Flame*, Vol. 122, pp. 139-150.

6. Renfro, M.W., Guttenfelder, W.A., King, G.B., and Laurendeau, N.M., 2000, "Scalar time-series measurements in turbulent $CH_4/H_2/N_2$ nonpremixed flames: OH," *Combustion and Flame*, Vol. 123, pp. 389-401.

7. Renfro, M.W., Gore, J.P., and Laurendeau, N.M., 2002, "Scalar time-series simulations using flamelet state relationships for turbulent non-premixed flames," *Combustion and Flame*, Vol. 129, pp. 120-135.

8. Renfro, M.W., Chaturvedy, A., King, G.B., Laurendeau, N.M., Kempf, A., Dreizler, A., and Janicka, J., 2004, "Comparison of OH time-series measurements and large-eddy simulations in hydrogen jet flames," *Combustion and Flame*, Vol. 139, pp. 142-151.

9. Zhang, J., Venkatesan, K.K., King, G.B., Laurendeau, N.M., and Renfro, M.W., 2005, "Two-point time-series measurements of minor-species concentrations in a turbulent nonpremixed flame," *Optical Letters*, Vol. 30, pp. 3144-3146.

10. Zhang, J., Venkatesan, K.K., King, G.B., Laurendeau, N.M., and Renfro, M.W., 2005, "Two-point OH time-series measurements in a nonpremixed turbulent jet flame," *Proceedings of the Fourth Joint U.S. Sections Meeting*, The Combustion Institute, Philadelphia, PA.

11. Pack, S.D., Renfro, M.W., King, G.B., and Laurendeau, N.M., 1998, "Photon-counting technique for rapid fluorescence-decay measurement," *Optics Letters*, Vol. 23, pp. 1215-1217.

12. TNF workshop, http://www.ca.sandia.gov/TNF.

13. Dibble, R.W., and Hollenbach, R.E., 1981, "Laser Rayleigh thermometry in turbulent flames," *Eighteenth Symposium (International) on Combustion*, The Combustion Institute, Pittsburg, pp. 1489-1499.

14. Ikeda, Y., Kojima, J., and Nakajima, T., 2000, "Local chemiluminescence measurements of OH*, CH* and C_2* at turbulent premixed flame-fronts," In *Smart Control of Turbulent Combustion*, Yoshida, A. (ed.), pp. 12-27.

15. Wang, G.H., Clemens, N.T., Varghese, P.L., 2005, "High-repetition rate measurements of temperature and thermal dissipation in a non-premixed turbulent jet flame," *Proceedings of the Combustion Institute.*, Vol. 30, pp. 691-699.

16. Hult, J., Meier, U., Meier, W., Harvey, A., and Kaminski, C.F., 2005, "Experimental analysis of local flame extinction in a turbulent jet diffusion flame by high repetition 2-D laser techniques and multi-scalar measurements," *Proceedings of the Combustion Institute.*,Vol. 30, pp. 701-709.

17. Landahl, M.T., and Mollo-Christensen, E., 1994, *Turbulence and Random Processes in Fluid Mechanics,* 2nd ed, Cambridge University Press, New York, NY.

18. Bergmann, V., Meier, W., Wolff, D., and Stricker, W., 1998, "Application of spontaneous Raman and Rayleigh scattering and 2D LIF for the characterization of a turbulent $CH_4/H_2/N_2$ jet diffusion flame," *Applied Physics B*, Vol. 66, pp. 489-502.

19. Barlow, R.S., and Karpetis, A.N., 2004, "Measurements of scalar variance, scalar dissipation, and length scales in turbulent piloted methane/air jet flames," *Flow Turbulence Combustion*, Vol. 72, pp. 427-448.

20. Seitzman, J.M., 1991, *Quantitative Applications of Fluorescence Imaging in Combustion*, PhD Thesis, Stanford University, Palo Alto, CA.

21. Zhang, J., King, G.B., Laurendeau, N.M., and Renfro, M.W., 2007, "Two-point time-series measurements of hydroxyl concentration in a turbulent nonpremixed flame," *Applied Optics*, Vol. 46 pp. 5742-5754.

22. Zhang, J., Venkatesan, K.K., King, G.B., Laurendeau, N.M., and Renfro, M.W., 2007, "Two-point OH time-series measurements in a nonpremixed turbulent jet flame," *Proceedings of the Fourth Joint U.S. Sections Meeting*, The Combustion Institute, Philadelphia, PA.

23. Wills, J.A.B., 1964, "On convection velocities in turbulent shear flows," *The Journal of Fluid Mechanics*, Vol. 20, pp. 417-432.

24. Ghenai, C., and Gökalp, I., 1998, "Correlation coefficients of the fluctuating density in turbulent premixed flames," *Experiments in Fluids*, Vol. 24, pp. 347-353.

25. Taylor, G.I., 1938, "The spectrum of turbulence," *Proceedings of the Royal Society A:*, Vol. 164, pp. 476-490.

26. Pope, S., 2000, *Turbulent Flows*, Cambridge University Press, Cambridge, UK.

27. Antonia, R.A., Browne, L.W.B., Rajagopalan, S., and Chambers, A.J., 1983, "On the organized motion of a turbulent plane jet," *Journal of Fluid Mechanics*, Vol. 134, pp. 49-66.